Optoelectronic synapses based on hot-electron-induced chemical processes

Pan Wang[†,], Mazhar E. Nasir, Alexey V. Krasavin, Wayne Dickson and Anatoly V. Zayats**

Department of Physics and London Centre for Nanotechnology, King's College London, Strand, London WC2R 2LS, UK

*Correspondence to: pan.wang@kcl.ac.uk, a.zayats@kcl.ac.uk

Abstract: Highly efficient information processing in brain is based on processing and memory components called synapses, whose output is dependent on the history of the signals passed through them. Here we have developed an artificial synapse with both electrical and optical memory effects using chemical transformations in plasmonic tunnel junctions. In an electronic implementation, the electrons tunnelled into plasmonic nanorods under low bias voltage are harvested to write information into the tunnel junctions via hot-electron-mediated chemical reactions with the environment. In an optical realization, the information can be written by external light illumination to excite hot electrons in plasmonic nanorods. The stored information is non-volatile and can be read either electrically or optically by measuring the resistance or inelastic-tunnelling-induced light emission, respectively. The described architecture provides high density (~10^{10} cm^{-2}) of memristive optoelectronic devices which can be used as multilevel nonvolatile memory, logic units or artificial synapses in future electronic, optoelectronic and artificial neural networks.

Keywords: Artificial synapse, plasmonic tunnel junction, hot electrons, memristor

Highly efficient information processing in brain utilises multilevel (as opposed to binary used in modern digital computers) electro-chemical logic components called synapses, which do not consume energy (non-volatile) while in a passive state. A memristive device (or memristor) is a resistive electrical element with resistance depending on the history of the applied electrical signals.[1,2] It can be used as a memory element for the storage of information or as an artificial synapse to emulate biological synapses in spiking neural networks (SNNs) as well as non-spiking artificial neural networks (ANNs).[3] Since the first experimental realization based on a metal/oxide/metal ($Pt/TiO_2/Pt$) structure[2], memristors have attracted extensive interest due to their important application in next-generation non-volatile memory, signal processing, reconfigurable logic devices, and neuromorphic computing[4-17]. Most of them rely on dynamically configuring the insulating layer under applied electric bias. To date, memristor realisations are typically based on two approaches relying on i) filament formation or annihilation upon control bias application in the insulating layers[7,14,16] and ii) spintronic devices based on magnetic tunnel junctions where the spin-polarised current leads to the movement of the magnetic domain walls[5,12,13,15]. In both realisations, the flowing current leads to the changes of the device resistance; however, in order to reverse the effect, the bias of opposite polarity needs to be applied. By integrating light-emitting or plasmonic properties with memristive devices, memristors with optical read-out have also been demonstrated (still requiring electric bias for changing the memristor state)[9,18-23], which are attractive for applications in optoelectronic or photonic systems. Recently, all-optical neuromorphic architecture based on the synapses made of phase-changing materials were demonstrated[8]. At the same time, the underlying feature of a biological synapse which changes resistivity depending on its chemical environment under the same polarity bias remains until now elusive.

Here, we demonstrate a general principle of operation of a new type of memristive devices acting as artificial synapses for non-spiking ANNs by taking advantage of the chemical transformations induced by hot-electrons in a tunnel junction. Using metal-polymer-metal tunnel junctions, we show the simultaneous multistate switching of the resistance and built-in light emission of the junctions, which is realized both electronically and optically by programming the junctions via hot-electron-mediated chemical reactions controlled by the environment. Since hot-electrons can be generated either electrically or optically and the tunnel junction has distinct electric response as well as acts as a nanoscale light source, the proposed approach allows several independent and interchangeable operation modalities in the same device with electronic (optical) programming and electronic (optical) readout, as well as electronic (optical) programming and optical (electronic) readout. Changing chemical (in this case gas) environment, an increased or decreased response or a nonvolatile state can be achieved under the bias of the same polarity.

A synapse is the functionalized junction between the axon of a presynapic neuron and the dendrite of a postsynapic neuron (Fig. 1a, left), which deals with the communications between neurons via neurotransmitters and acts as both the computing and the memory unit. Light-emitting tunnel junction (Fig. 1a, right), an optoelectronic analog of a biological synapse, was constructed based on a plasmonic nanorod. During the tunnelling process (Fig. 1b), the inelastically tunneled electrons excite plasmons in the nanorod which can subsequently decay radiatively into photons, while those electrons that tunnel elastically, generate hot electrons in the tips of nanorods which can be harvested for inducing chemical reaction in a chosen gas environment, which will influence the resistivity of the tunnel junction. In this way, the multilevel writing of the junction state can be achieved by changing the gas environment to promote oxidation or reduction reactions or to keep non-reactive state under the applied bias. In the latter

case, the information stored is non-volatile and can be read both electrically and optically by interrogating the resistance and emission intensity. In this sense, the light-emitting tunnel junction is a direct analogue of a biological synapse where the resistance between the axon and the dendrite is adjustively controlled by the release of the chemical species and the strength of the transmitted signal. Similarly, in the proposed artificial synapse, the tunneling resistance of the junction is controlled by the introduction of gas in conjunction with the strength of the passing tunneling current. Optical coding of the tunnel junctions is also possible using the hot-electrons generated in the tunnel junctions by an external illumination in the respective gas environments.

Experimentally, tunnel junctions were constructed in a plasmonic nanorod array (Fig. 1c), which was fabricated by electrodeposition of Au into porous alumina templates (see Supplementary Section 1). Figure 1d presents the cross-sectional view of a plasmonic nanorod array, clearly showing the Au nanorods embedded in the alumina template. The diameter, length, and separation of the nanorods are approximately 65, 480, and 105 nm, respectively. Metal-polymer-metal tunnel junctions were constructed on the surface of the nanorod metamaterial by using a monolayer of poly-L-histidine (PLH) as the tunnel barrier and 'storage' layer (used as a reactant to store information via reconfigurable chemical reactions), and a droplet of eutectic gallium indium (EGaIn) as the top electrode (see Supplementary Section 2 for details). Each Au nanorod forms a tunnel junction with the top EGaIn contact (Fig. 1a), creating an array of tunnel junctions (Supplementary Section 3) with density determined by the density of Au nanorods in the metamaterial on the order of $\sim 10^{10}$ cm^{-2} (estimated from the SEM image shown in Figure S1). Nonlinear character of current-voltage characteristic (Fig. 1e) confirms the tunnelling of electrons through the metal-polymer-metal junctions[24]. Upon the application of a forward bias, light emission was observed from the substrate side of the device, which is due to the radiative decay of plasmons excited in

the nanorod metamaterial[25-30] (Fig. 1b). The recorded emission spectra (having a linewidth of ~200 nm) as a function of the applied bias are shown in Fig. 1f. With the increase of the bias, the emission intensity increases gradually, accompanied by a blue-shift of the emission peaks following the quantum cut-off law $h\nu_{photon} \leq eV_b$.[25] The spectrum of the emission is determined by the product of the emission power spectrum of the fluctuating tunneling current, the modal profile of the metamaterial and the radiation efficiency of the excited modes[31]. The electron-to-photon conversion efficiency is estimated to be around 10^{-6}, which is determined by the radiation efficiency (~3.5×10^{-4}, Supplementary Section 4) of the metamaterial, and can be improved by engineering the local density of optical states and radiation efficiency of the tunnel junctions[31].

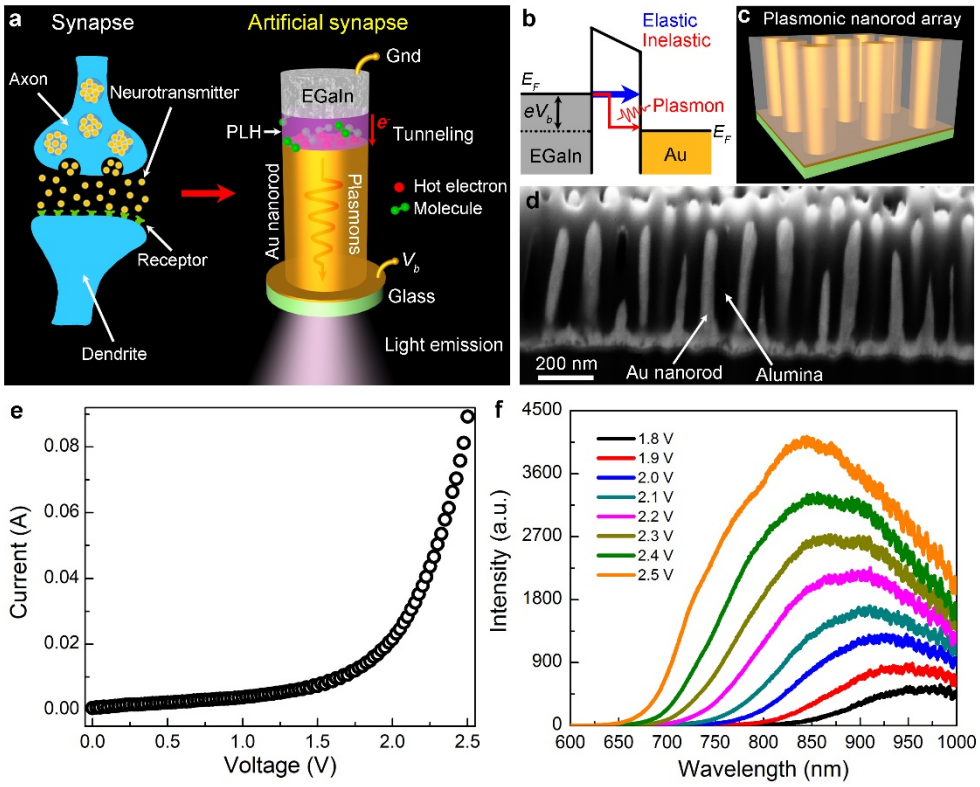

Figure 1 | Memristor structure and light emission properties. a, Schematic diagram of the memristive light-emitting tunnel junction, which is an optoelectronic analogue to a synapse (EGaIn and PLH denote eutectic

gallium indium and poly-L-histidine, respectively). **b**, An energy level diagram of the tunnel junction with a bias of V_b. **c**, Schematic diagram of the plasmonic nanorod array used to realize multiple tunnel junctions. **d**, Cross-sectional SEM view of a nanorod array. **e**, Measured current-voltage characteristic of a tunnelling device fabricated using the array shown in **d**. **f**, Measured emission spectra of the tunnelling device as a function of the applied forward bias.

During the tunnelling process, the majority of electrons (~99%) tunnel elastically (Fig. 1b)[24–29], appearing as hot electrons[32,33] in the tips of Au nanorods, which can be used for programming the state of the tunnel junctions via hot-electron-activated chemical reactions[34,35]. To use the hot-electron effects, the tunnelling device was put into a gas chamber under a bias of 2.5 V, with the tunnelling current and emission spectrum monitored simultaneously. The device was first stabilized in 2% H_2 in N_2, then, upon switching of a chamber environment to air, the tunnelling current decreased gradually down to two thirds of the original value (Fig. 2a). At the same time, the integrated light emission intensity increased gradually to twice the original value. The changes in the tunnelling current and emission intensity reflect a change in the junction state, which is due to the oxidization of the tunnel junctions by oxygen molecules in air mediated by hot electrons as a PLH monolayer undergoes oxidative dehydrogenation and coupling reactions[30].

The resistance and emission intensity of the tunnelling device depend on the total number of the tunneled electrons (Fig. 2b) since the state of tunnel junctions is dependent on the history of the tunnelling process, particularly on how many electrons have traversed the junctions before, demonstrating the memory effect similar to biological synapses. During the reaction, the device was brought from a low resistance state (~20 Ω) to a high resistance state (~29 Ω), with a simultaneous change in the light emission from a low intensity to high intensity state (~80% increase in intensity). In

this case, the written state of the tunnel junctions can be read out both electrically and optically, which is attractive for use as memory devices or artificial synapses, not only in electronic but also in optoelectronic systems. Moreover, compared with the existing optical memristors which require external light sources for the optical readout[19–22,36], the plasmonic tunnel junctions have nanoscale built-in plasmonic light sources, providing advantage for the dramatic reduction in the device size and power consumption (the operation power for single tunnel junction is around 600 pW, see Supplementary Section 4 for details). Normally, the emission intensity changes linearly with the tunnelling current, however, the emission intensity shows an opposite trend to that of the current during the reaction. This can be understood considering the evolution of the estimated inelastic tunnelling efficiency during the programming process (Fig. 2c, see Supplementary Section 5 for details). During the reaction of the tunnel junctions with oxygen molecules, the inelastic tunnelling efficiency increases gradually, resulting in the increased light emission intensity despite the gradual decrease of the tunnelling current.

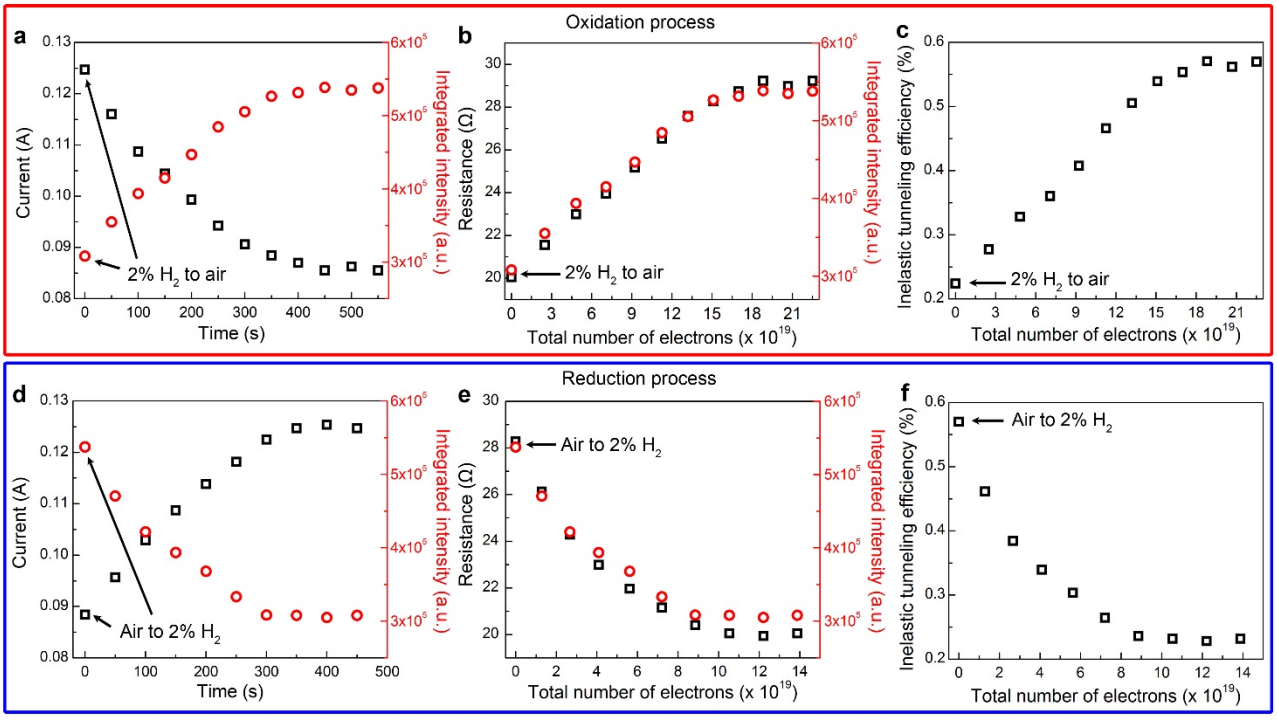

Figure 2 | Hot-electron-mediated programming of electrical and optical properties. a, Time-dependent evolution of the tunnelling current and integrated emission intensity during the hot-electron-mediated reaction of tunnel junctions with oxygen (environment switched from 2% H_2 gas to air). **b**,**c**, Dependence of the resistance and integrated emission intensity (**b**), and the inelastic tunnelling efficiency (**c**) on the total number of the tunneled electrons. **d**, Time-dependent evolution of the tunnelling current and integrated emission intensity during the hot-electron-mediated reaction of oxidized tunnel junctions with hydrogen (environment switched from air to 2% H_2). **e**,**f**, Dependence of the resistance and integrated emission intensity (**e**), and the inelastic tunnelling efficiency (**f**) on the total number of the tunneled electrons. V_b is fixed at 2.5 V in all the measurements.

The tunnelling device can be programmed back to the original status by introducing hydrogen molecules into the cell via the hot-electron-mediated reduction of the oxidized tunnel junctions (Fig. 2d–f). The resistance, integrated emission intensity, and inelastic tunnelling efficiency (Fig. 2e,f) decreased gradually back to the original value with the continuous supply of the hot electrons and hydrogen molecules, highlighting the ability to reversibly programme the tunnelling device. The dynamics of the light-emitting reactive tunnel junctions can be associated with long-term potentiation/depression processes of synapses in a biological neural network. Different from ferroelectric or magnetic tunnel junction based memristors exploiting tunnel electroresistance or magnetoresistance effects[12,13], the light-emitting plasmonic tunnel junctions exploit elastically tunneled electrons for the writing of information and inelastically tunneled electrons for the optical readout, providing programmability of the response and sensitivity to the environment. It is worth noting that, the relatively long time taken for the writing of information (Fig. 2a and 2d) is due to the slow diffusion of gas molecules into the large-area highly-confined tunnel junction array, which should be improved by reducing the surface area of the

device or patterning the device into crossbar structure for the quicker diffusion of gases into the junctions.

As discussed above, the state of the tunnel junctions is highly dependent on the number of the tunneled electrons and the environment. By controlling the supply of hot electrons or reactants (oxygen or hydrogen), the tunnelling device can be latched to different intermediate states. For example, as shown in Fig. 3a, the resistance of the device was switched from ~20 Ω (low resistance state, level L) to 22 (level 1), 26 (level 2), and 29 Ω (high resistance state, level H), respectively, by controllably introducing oxygen molecules into the chamber for the oxidization of the tunnel junctions. When the required state was achieved, pure nitrogen (employed as a nonreactive environment) was introduced into the chamber to remove oxygen molecules to latch the state of the junctions. Under the nonreactive environment of nitrogen, the state of the junctions was maintained when the bias was switched off (see Supplementary Section 6), showing the non-volatility. Accordingly, the light emission from the device was also latched to different intermediate levels (Fig. 3b). The slight shift in the emission peak is due to the modification of the local density of optical states in the junctions by the chemical reactions. Benefitted from the programming mechanism of the reactive tunnel junctions, the states of the junctions may, in principle, be controlled on single electron or molecule level. Therefore, the number of levels can be regulated by either the tunneling current (therefore, a bias), the interaction time and even the quantity of reactive gases introduced into the junctions, with maximum number ultimately determined by the noise in the readout signal. Instead of carrying out computations based on binary in digital chips, the artificial synapses based on reactive tunnel junctions work in an analog way like neurons in brain that activate in various way depending on the type and number of ions that flow across a synapse.

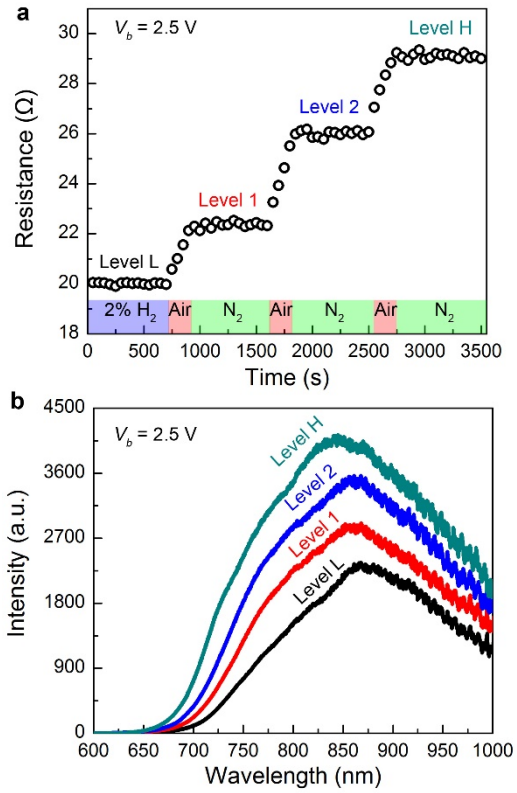

Figure 3 | Multilevel programming of the electrical and optical properties. a, Continuous switching of the resistance of the tunnelling device by controlling the environment. The device was first stabilized in 2% H_2 (V_b = 2.5 V), then the resistance was switched by the introduction of oxygen molecules and latched by replacing oxygen environment with nitrogen. **b**, Corresponding latched emission spectra of the tunnelling device.

Apart from the eletrochemical programming, the state of the tunnel junctions can be programmed optically. Under external light illumination of the nanorod metamaterial from the substrate side, the plasmonic modes in the metamaterial are excited. Figure 4a shows the simulated electric field and current distributions in the unit cell of the metamaterial illuminated by light with a wavelength of 600 nm at which the extinction has a maximum (see Supplementary Section 7 for details). The plasmonic excitation exists across the whole nanorod length and hot electrons are generated not only at the side-walls in the lower part of the nanorods but also at the tips of the Au nanorods, the latter can be used

directly for the activation of chemical reactions in the tunnel junctions.[37] In order to demonstrate this (Fig. 4b), the device was first stabilized in 2% H_2 in N_2 under 2.5 V (period 1). The state of the junctions was unchanged when the environment was switched to air under zero bias (period 2) due to the lack of hot electrons for the reaction (under applied bias the gradual rise of the tunnel resistance to level H was observed as expected (period 3)). The state was programmed back to the low resistance level (period 4) by introducing 2% H_2 back into the chamber under applied bias. However, when the environment was switched to air under zero bias but the metamaterial was illuminated by a broadband light (500-750 nm, matched with the extinction peak) with a power density of ~0.02 W/cm^2 (period 5), the state of the junctions was programmed to the high resistance level (confirmed by the stable resistance after the removal of illumination under a bias of 2.5 V (period 6)). The spectra of latched light emission correspond to the level L and optically switched level H' agree well with the emission spectra from the electrically programmed low and high resistance levels (cf., Fig. 4c and Fig. 3b). The ability of optical coding provides an alternative choice for the writing of information with advantages such as wireless and wavelength-dependent control.

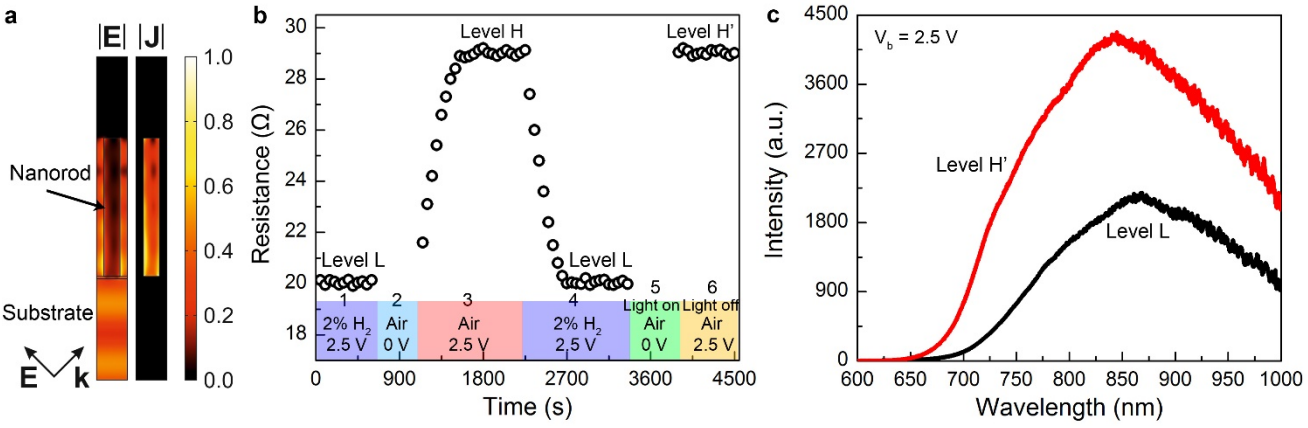

Figure 4 | Optical programming of the tunnelling device. a, Normalized simulated electric field |E| and current |J|

distributions in the unit cell of the metamaterial for illuminated by light with a wavelength of $\lambda = 600$ nm. **b**, Evolution of the resistance of the tunnelling device under different conditions as indicated at the bottom. White light illumination in the spectral range 500-750 nm and power density ~0.03 W cm^{-2} was used during period 5. **c**, Emission spectra of the tunnelling device measured at the resistance level L and the optically programmed resistance level H'.

In conclusion, we have investigated the electrical and optical memory effects in reactive plasmonic tunnel junctions. The high density of tunnel junctions (~10^{10} cm^{-2}) and scalability provided by the plasmonic nanorod array make the proposed approach a promising platform for the construction of neuromorphic computing devices. Direct analogy can be considered of multiple tunnel junctions connected to the same back electrode emulating multiple biological synapses connected to a neuron. Additionally, by patterning the nanorod array[38] and the top electrodes into micro or nanoscale crossbars[6,7], it is possible to configure the plasmonic nanorod array into a network of tunnel junction units formed at each crosspoint which can be addressed individually with both electrical and optical approaches (despite of the global gas environment, the information is written only when individual units are addressed, local gas environment can be achieved using a nanotube geometry instead of nanorod[39]). The proposed programmable tunnel junctions may be applied as both a memristive multilevel devices in traditional electronic circuits as well artificial synapses for non-spiking ANNs. The light-emitting reactive tunnel junctions can also be integrated directly with plasmonic or silicon waveguides to deliver or collect optical signals for the application as memory, logic units, and artificial synapses in optoelectronic systems, scaled down to single junctions if required.

ASSOCIATED CONTENT

Supporting Information

The Supporting Information is available free of charge on the ACS Publications website at DOI: .

Fabrication of plasmonic nanorod metamaterials; fabrication of metal-polymer-metal tunnel junctions; nanorod-metamaterial-based tunnelling device; estimation of inelastic tunnelling efficiency; non-volatility of the device; numerical simulations,

AUTHOR INFORMATION

Corresponding Author

*Email: pan.wang@kcl.ac.uk, a.zayats@kcl.ac.uk

Present Address

†State Key Laboratory of Modern Optical Instrumentation, College of Optical Science and Engineering, Zhejiang University, Hangzhou 310027, China.

Notes

The authors declare no competing financial interests.

Acknowledgments

This work has been funded in part by the Engineering and Physical Sciences Research Council (UK) and the European Research Council iPLASMM project (321268). A.V.Z. acknowledges support from the Royal Society and the Wolfson Foundation.

References

1. Chua, L. O. Memristor-the missing circuit element. *IEEE Trans. Circuit Theory* ***18,*** 507–519 (1971).
2. Strukov, D. B., Snider, G. S., Stewart, D. R. & Williams, R. S. The missing memristor found. *Nature* ***453,*** 80–83 (2008).
3. Jeong, H. & Shi, L. P. Memristor devices for neural networks. *J. Phys. D: Appl. Phys.* **52,** 023003 (2019).
4. Yang, J. J., Strukov, D. B. & Stewart, D. R. Memristive devices for computing. *Nat. Nanotechnol.* ***8,*** 13–24 (2013).
5. Parkin, S. & Yang, S. -H. Memory on the racetrack. *Nat. Nanotechnol.* **10,** 195–198 (2015).
6. Zidan, M. A., Strachan, J. P. & Lu, W. D. The future of electronics based on memristive systems. *Nat. Electron.* ***1***, 22–29 (2018).
7. Yang, J. J., Pickett, M. D., Li, X. M., Ohlberg, D. A. A., Stewart, D. R. & Williams, R. S. Memristive switching mechanism for metal/oxide/metal nanodevices. *Nat. Nanotechnol.* ***3,*** 429–433 (2008).
8. Li, C., Hu, M., Li, Y. N., Jiang, H., Ge, N., Montgomery, E., Zhang, J. M., Song, W. H., Davila, N., Graves, C. E., Li, Z. Y., Strachan, J. P., Lin, P., Wang, Z. R., Barnell, M., Wu, Q., Williams, R. S., Yang, J. J. & Xia, Q. F. Analogue signal and image processing with large memristor crossbars. *Nat. Electron.* ***1,*** 52–59 (2018).
9. Feldmann, J., Youngblood, N., Wright, C. D., Bhaskaran, H. & Pernice, W. H. P. All-optical spiking neurosynaptic networks with self-learning capabilities. *Nature* **569**, 208-214 (2019).
10. Borghetti J., Snider, G. S., Kuekes, P. J., Yang, J. J., Stewart, D. R. & Williams, R. S. ‘Memristive’ switches enable ‘stateful’ logic operations via material implication. *Nature* ***464,*** 873–876 (2010).

11. Jo, S. H., Chang, T., Ebong, I., Bhadviya, B. B., Mazumder, P. & Lu, W. Nanoscale memristor device as synapse in neuromorphic systems. *Nano Lett.* ***10,*** 1297–1301 (2010).

12. Krzysteczko, P., Münchenberger, J., Schäfers, M., Reiss, G., Thomas, A. The memristive magnetic tunnel junction as a nanoscopic synapse-neuron system. *Adv. Mater.* ***24,*** 762–766 (2012).

13. Kim, D. J., Lu, H., Ryu, S., Bark, C. -W., Eom, C. -B., Tsymbal, E. Y. & Gruverman, A. Ferroelectric tunnel memristor. *Nano Lett.* **12,** 5697–5702 (2012).

14. Wu, C. X., Kim T. W., Choi H. Y., Strukov D. B. & Yang J. J. Flexible three-dimensional artificial synapse networks with correlated learning and trainable memory capability. *Nat. Commun.* **8,** 752 (2017).

15. Schneider, M. L., Donnelly, C. A., Russek, S. E., Baek, B., Pufall, M. R., Hopkins, P. F., Dresselhaus, P. D., Benz, S. P. & Rippard, W. H. Ultralow power artificial synapses using nanotextured magnetic Josephson junctions. *Sci. Adv.* **4,** e1701329 (2018).

16. Choi, S., Tan, S. H., Li, Z. F., Kim, Y., Choi, C., Chen, P. -Y., Yeon, H., Yu, S. M. & Kim, J. SiGe epitaxial memory for neuromorphic computing with reproducible high performance based on engineered dislocations. *Nat. Mater.* **17,** 335–340 (2018).

17. Moon, K., Lim, S., Park, J., Sung, C., Oh, S., Woo, J. & Hwang, H. RRAM-based synapse devices for neuromorphic systems. Faraday Discuss. 213, 421–451 (2019).

18. He, C. L., Li, J. F., Wu, X., Chen, P., Zhao, J., Yin, K. B., Cheng, M., Yang, W., Xie, G. B., Wang, D. M., Liu, D. H., Yang, R., Shi, D. X., Li, Z. Y., Sun, L. T. & Zhang, G. Y. Tunable electroluminescence in planar graphene/SiO_2 memristors. *Adv. Mater.* **25,** 5593–5598 (2013).

19. Emboras, A., Goykhman, I., Desiatov, B., Mazurski, N., Stern, L., Shappir, J. & Levy, U. Nanoscale plasmonic memristor with optical readout functionality. *Nano Lett.* **13,** 6151–6155 (2013).

20. Lei, D. Y., Appavoo, K., Ligmajer, F., Sonnefraud, Y., Haglund, R. F., Jr. & Maier, S. A. Optically-triggered nanoscale memory effect in a hybrid plasmonic-phase changing nanostructure. *ACS Photon.* **2,** 1306–1313 (2015).
21. Emboras, A., Niegemann, J., Ma, P., Haffner, C., Pedersen, A., Luisier, M., Hafner, C., Schimmel, T. & Leuthold, J. Atomic scale plasmonic switch. *Nano Lett.* **16,** 709–714 (2016).
22. Martino, G. D. & Tappertzhofen, S. Optically accessible memristive devices. Nanophotonics. DOI:10.1515/nanoph-2019-0063 (2019).
23. Cheng, Z. G., Ríos, C., Pernice ,W. H. P., Wright, C. D. & Bhaskaran, H. On-chip photonics synapse. *Sci. Adv.* **3,** e1700160 (2017).
24. Simmons, J. G. Generalized formula for the electric tunnel effect between similar electrodes separated by a thin insulating film. *J. Appl. Phys.* **34,** 1793–1803 (1963).
25. Lambe, J. & McCarthy, S. L. Light emission from inelastic electron tunneling. *Phys. Rev. Lett.* **37,** 923–925 (1976).
26. Kern, J., Kullock, R., Prangsma, J., Emmerling, M., Kamp, M. & Hecht, B. Electrically driven optical antennas. *Nat. Photon.* **9,** 582–586 (2015).
27. Parzefall, M., Bharadwaj, P., Jain, A., Taniguchi, T., Watanabe, K. & Novotny, L. Antenna-coupled photon emission from hexagonal boron nitride tunnel junctions. *Nat. Nanotechnol.* **10,** 1058–1063 (2015).
28. Du, W., Wang, T., Chu, H. -S., Wu, L., Liu, R. R., Sun, S., Phua, W. K., Wang, L. J., Tomczak, N. & Nijhuis, C. A. On-chip molecular electronic plasmon sources based on self-assembled monolayer. *Nat. Photon.* **10,** 274–280 (2016).

29. Du, W., Wang, T., Chu, H. –S. & Nijhuis, C. A. Highly efficient on-chip direct electronic-plasmonic transducers. *Nat. Photon.* **11,** 623–627 (2017).

30. Wang, P., Krasavin, A. V., Nasir, M. E., Dickson, W. & Zayats, A. V. Reactive tunnel junctions in electrically driven plasmonic nanorod metamaterials. *Nat. Nanotechnol.* **13,** 159–164 (2018).

31. Qian, H. L., Hsu, S. -W., Gurunatha, K., Riley, C. T., Zhao, J., Lu, D., Tao, A. R. & Liu, Z. W. Efficient light generation from enhanced inelastic electron tunnelling. *Nat. Photon.* **12,** 485–488 (2019).

32. Brongersma, M. L., Halas, N. J. & Nordlander, P. Plasmon-induced hot carrier science and technology. *Nat. Nanotech.* **10,** 25–34 (2015).

33. Harutyunyan, H., Martinson, A. B. F., Rosenmann, D., Khorashad, L. K., Besteiro, L. V., Govorov, A. O. & Wiederrecht, G. P. Anomalous ultrafast dynamics of hot plasmonic electrons in nanostructures with hot spots. *Nat. Nanotechnol.* **10,** 770–774 (2015).

34. Mubeen, S., Lee, J., Singh, N., Kramer, S., Stucky, G. D. & Moskovits, M. An autonomous photosynthetic device in which all charge carriers derive from surface plasmons. *Nat. Nanotechnol.* **8,** 247–251 (2013).

35. Zhai, Y. M., DuChene, J. S., Wang, Y. -C., Qiu, J. J., Johnston-Peck, A. C., You, B., Guo, W. X., DiCiaccio, B., Qian, K., Zhao, E. W., Ooi, F., Hu, D. H., Su, D., Stach, E. A., Zhu, Z. H. & Wei, W. D. Polyvinylpyrrolidone-induced anisotropic growth of gold nanoprisms in plasmon-driven synthesis. *Nat. Mater.* **15,** 889–895 (2016).

36. Hoessbacher, C., Fedoryshyn, Y., Emboras, A., Melikyan, A., Kohl, M., Hillerkuss, D., Hafner, C. & Leuthold, J. The plasmonic memristor: a latching optical switch. *Optica* **1,** 198–202 (2014).

37. Ho, K. H. W., Shang, A. X., Shi, F. H., Lo, T. W., Yeung, P. H., Yu, Y. S., Zhang, X. M., Wong, K. -Y., Lei, D. Y. Plasmonic Au/TiO2-dumbbell-on-film nanocavities for high-efficiency hot-carrier generation and extraction. *Adv. Funct. Mater.* **28,** 1800383 (2018).

38. Dickson, W., Beckett, S., McClatchey, C., Murphy, A., O'Connor, D., Wurtz, G. A., Pollard, R. & Zayats, A. V.Hyperbolic polaritonic crystals based on nanostructured nanorod metamaterials. *Adv. Mater.* **27,** 5974–5980 (2015).

39. McPhillips, J., Murphy, A., Jonsson, M. P., Hendren, W. R., Atkinson, R., Hook, F., Zayats, A. V. & Pollard, R. High-performance biosensing using arrays of plasmonic nanotubes. *ACS Nano* **4,** 2210–2216 (2010).

Table of Contents Graphic